A halo-independent lower bound on the dark matter capture rate in the Sun from a direct detection signal

Journal of Cosmology and Astroparticle Physics
An IOP and SISSA journal

A halo-independent lower bound on the dark matter capture rate in the Sun from a direct detection signal

Mattias Blennow,[a] **Juan Herrero-Garcia**[a] **and Thomas Schwetz**[b]

[a]Department of Theoretical physics, School of Engineering Sciences,
KTH Royal Institute of Technology,
AlbaNova University Center, 106 91 Stockholm, Sweden
[b]Oskar Klein Centre for Cosmoparticle Physics, Department of Physics,
Stockholm University,
SE-10691 Stockholm, Sweden

E-mail: emb@kth.se, juhg@kth.se, schwetz@fysik.su.se

Received February 16, 2015
Revised April 27, 2015
Accepted May 5, 2015
Published May 21, 2015

Abstract. We show that a positive signal in a dark matter (DM) direct detection experiment can be used to place a lower bound on the DM capture rate in the Sun, independent of the DM halo. For a given particle physics model and DM mass we obtain a lower bound on the capture rate independent of the local DM density, velocity distribution, galactic escape velocity, as well as the scattering cross section. We illustrate this lower bound on the capture rate by assuming that upcoming direct detection experiments will soon obtain a significant signal. When comparing the lower bound on the capture rate with limits on the high-energy neutrino flux from the Sun from neutrino telescopes, we can place upper limits on the branching fraction of DM annihilation channels leading to neutrinos. With current data from IceCube and Super-Kamiokande non-trivial limits can be obtained for spin-dependent interactions and direct annihilations into neutrinos. In some cases also annihilations into $\tau\tau$ or bb start getting constrained. For spin-independent interactions current constraints are weak, but they may become interesting for data from future neutrino telescopes.

Keywords: dark matter theory, dark matter experiments

ArXiv ePrint: 1502.03342

doi:10.1088/1475-7516/2015/05/036

JCAP05(2015)036

Contents

1 Introduction

From gravitational effects we know that dark matter (DM) constitutes a significant fraction of the energy density of the Universe. Among the most promising ways to search for non-gravitational manifestations of DM particles are direct detection (DD) experiments, which are looking for the scattering of DM particles from the galactic halo in underground detectors [1–8], and neutrino telescopes looking for high-energy neutrinos from the annihilations of DM particles in the Sun [9–13]. The latter signal emerges from the capture of galactic DM particles in the gravitational potential of the Sun after loosing enough energy in a DM-nucleus scattering event in the Sun. Hence, the capture rate of DM in the Sun is determined by the scattering cross section of the DM particle on nuclei, the same process which provides the signal in DD experiments. The resulting neutrino flux from the Sun will also depend on the annihilation channels of the DM particle. Therefore, viable information on DM properties can in principle be obtained by comparing the two signals.

However, the DD signal and the DM capture in the Sun depend on different parts of the DM velocity distribution. While DD experiments are sensitive to DM particles with velocity larger than a certain minimal velocity (which depends on the mass of the nuclei in the detector and its energy threshold as well as on the DM mass), the DM capture in the Sun is sensitive to values below a certain maximum velocity, above which capture of DM particles is kinematically forbidden. Therefore, in order to explore the complementarity of the two signals, it is common to adopt specific DM velocity distributions, for instance the so-called Standard Halo Model (SHM) consisting of a truncated Maxwellian distribution, see

JCAP05(2015)036

refs. [14–21] for a very incomplete list of examples of this approach. However, the properties of the DM velocity distribution as well as the local DM density are plagued with large uncertainties and halo-independent methods are desirable to draw robust conclusions about possible signals. The impact of variations of halo properties on the neutrino signal have been studied for instance in refs. [22, 23] and in the context of the neutrino/DD comparison in ref. [24]. The authors of ref. [25] investigated the potential to extract DM parameters from a combination of data from DD experiments and from a neutrino signal based on a polynomial parameterization of the DM velocity distribution, whose parameters are fitted together with the DM parameters.

In the present paper we develop a completely halo-independent method to compare a signal from a DD experiment with a neutrino signal from the Sun. We show that from a precise measurement of the DD nuclear recoil spectrum a halo-independent lower bound on the capture rate in the Sun can be derived. It is based on the overlap region in velocity space and therefore does not require any assumptions about the halo properties. Our bound extends the halo-independent methods developed in the context of DD [26, 27] to the capture rate in the Sun.

The remainder of this paper is organized as follows: we review the phenomenology of DD in section 2 and of the DM induced neutrino signal from the Sun in section 3. We then discuss the relation of direct detection to the capture rate in the Sun in section 4, where the central result of the paper (the lower bound on the capture rate) is given in section 4.2. In section 5, we apply the bound to mock data from future direct detection experiments and compare them to the upper bounds from the IceCube and Super-Kamiokande neutrino telescopes. We also comment on the importance of nuclear form factor uncertainties as well as on the ratio of the neutron and proton couplings. We summarize and give our concluding remarks in section 6. In appendix A, we discuss how to use an annual modulation signal in a DD experiment to provide the lower bound on the capture rate, and apply our results to the DAMA signal. In appendix B we show how to use our results in the case of more general scattering cross sections, beyond contact interactions.

2 Dark matter direct detection

In this section we review the relevant expressions for DD of dark matter [28]. We focus on elastic scattering of DM particles χ with mass m_χ off a nucleus with mass number A and mass m_A, depositing the nuclear recoil energy E_R. The differential rate (measured in events/keV/kg/day) for a single target detector is:[1]

$$\mathcal{R}(E_R,t) = \frac{\rho_\chi}{m_\chi m_A}\int_{|\vec{v}|>v_m} d^3v\, v f_{\rm det}(\vec{v},t)\frac{d\sigma_A}{dE_R}(v)\,, \tag{2.1}$$

with ρ_χ being the local DM mass density and v_m is the minimal velocity of the DM particle required for a recoil energy E_R:

$$v_m = \sqrt{\frac{m_A E_R}{2\mu_{\chi A}^2}}\,, \tag{2.2}$$

[1]For detectors with several nuclei the total rate is the sum of the rates in all nuclei, i.e., $\mathcal{R}(E_R,t) = \sum_A \mathcal{R}_A(E_R,t)$, but usually one nucleus gives the dominant contribution to the rate for a particular DM mass.

JCAP05(2015)036

where $\mu_{\chi A}$ is the reduced mass of the DM-nucleus system. The function $f_{\rm det}(\vec{v},t)$ describes the distribution of DM particle velocities in the detector rest frame, with the normalization

$$\int d^3v\, f_{\rm det}(\vec{v},t) = \int_0^\infty dv\, v^2 \tilde{f}_{\rm det}(v,t) = 1\,, \tag{2.3}$$

and we define the angular averaged velocity distribution function $\tilde{f}$ by

$$\tilde{f}(v) \equiv \int d\Omega f(v,\Omega)\,, \tag{2.4}$$

where $d\Omega = d\cos\theta\, d\phi$. The velocity distributions in the rest frames of the detector, the Sun and the galaxy are related by $f_{\rm det}(\vec{v},t) = f_{\rm Sun}(\vec{v}+\vec{v}_e(t)) = f_{\rm gal}(\vec{v}+\vec{v}_s+\vec{v}_e(t))$, where $\vec{v}_e(t)$ is the velocity vector of the Earth relative to the Sun and $\vec{v}_s$ is the velocity of the Sun relative to the galactic frame. The revolution of the Earth around the Sun encoded in $\vec{v}_e(t)$ leads to an annual modulation of the DD signal [29, 30].

To be specific, in the following we will concentrate on spin-independent (SI) and spin-dependent (SD) scattering from a contact interaction. This implies that the differential scattering cross section $d\sigma_A(v)/dE_R$ scales as $1/v^2$. Our results can also be generalized to other v dependences, as shown in appendix B. For SI contact interactions with equal DM couplings to neutrons and protons the cross section becomes

$$\frac{d\sigma_A}{dE_R}(v) = \frac{m_A \sigma_\chi^p A^2}{2\mu_{\chi p}^2 v^2} F_A^2(E_R)\,, \tag{2.5}$$

where σ_χ^p is the total DM-proton scattering cross section at zero momentum transfer, $\mu_{\chi p}$ is the DM-proton reduced mass, and $F_A(E_R)$ is a nuclear form factor. For SD interactions a similar formula applies with no A^2 enhancement and a different form factor.

Then the event rate eq. (2.1) becomes

$$\mathcal{R}(E_R,t) = A^2 F_A^2(E_R)\, \tilde{\eta}(v_m,t)\,, \tag{2.6}$$

where v_m is considered as a function of E_R according to eq. (2.2) and we have defined

$$\tilde{\eta}(v_m,t) \equiv \mathcal{C}\,\eta(v_m,t) \quad \text{with} \quad \eta(v_m,t) \equiv \int_{v_m}^\infty dv\, v \tilde{f}_{\rm det}(v,t) \quad \text{and} \quad \mathcal{C} \equiv \frac{\rho_\chi \sigma_\chi^p}{2 m_\chi \mu_{\chi p}^2}\,. \tag{2.7}$$

Notice that $\tilde{\eta}$ depends only on the DM properties and the DM halo, but is independent of the characteristics of the experiment. For fixed DM mass, one can translate the event rate in E_R space into v_m space, and $\tilde{\eta}(v_m,t)$ then has to be the same for any experiment. This is the basis of the halo-independent methods developed in refs. [26, 27] and used extensively to compare results of different DD experiments, see, e.g., refs. [31–42].

For a specific detector the number of DM induced events in an energy range between E_1 and E_2 is given by

$$N_{[E_1,E_2]} = MTA^2 \int_0^\infty dE_R\, F_A^2(E_R) G_{[E_1,E_2]}(E_R) \tilde{\eta}(v_m,t)\,, \tag{2.8}$$

where M and T are the detector mass and exposure time respectively, and $G_{[E_1,E_2]}(E_R)$ is the detector response function describing the probability that a DM event with true recoil energy

JCAP05(2015)036

E_R is reconstructed in the observed energy interval $[E_1, E_2]$, including energy resolution, energy dependent efficiencies, and possibly also quenching factors.

In section 4.2 we will assume that a positive signal is observed in a direct detection experiment. In this case, the angular averaged distribution $\tilde{f}(v)$ times the constant $\mathcal{C}$ can be extracted from the data (modulo experimental resolutions and uncertainties). Using eqs. (2.6) and (2.7), we find [43]

$$\mathcal{C}\tilde{f}(v) = -\frac{1}{v}\frac{d\tilde{\eta}(v)}{dv} = -\frac{1}{vA^2}\frac{d}{dv}\left(\frac{\mathcal{R}(E_R)}{F_A^2(E_R)}\right), \tag{2.9}$$

where E_R is considered as a function of $v = v_m$ according to eq. (2.2), depending on the DM mass.

3 The neutrino signal from DM annihilations in the Sun

In this section we briefly review the relevant expressions for the neutrino signal from the Sun. Due to the scattering of DM particles with the nuclei in the Sun they may lose energy and become gravitationally bound to the Sun. Their annihilation products can produce neutrinos with energies comparable to the DM mass, detectable at Earth [44–46].

The capture rate of dark matter particles is given by (see, e.g., refs. [46, 47])

$$C_{\rm Sun} = 4\pi\frac{\rho_\chi}{m_\chi}\sum_A \int_0^{R_{\rm Sun}} dr\, r^2 \int_0^\infty dv \tilde{f}(v)\, v\, w\, \Omega_A(w, r)\,, \tag{3.1}$$

where, for SI interactions, the sum over A goes over all element abundances in the Sun up to nickel, while for SD interactions only hydrogen is relevant. We use the short-hand notation $\tilde{f}_{\rm Sun} \equiv \tilde{f}$ and the angular averaged velocity distribution function is defined in eq. (2.4). The function $\tilde{f}(v)$ refers to the velocity distribution at infinity, whereas w is the DM velocity inside the gravitational potential of the Sun at the radial distance r from the solar center, given by $w^2 = v^2 + u_{\rm esc}^2(r)$, with $u_{\rm esc}^2(r)$ being the escape velocity from the Sun depending on the location r. The quantity $\Omega_A(w, r)$ is the rate with which a DM particle with velocity w will be gravitationally captured by scattering on the nucleus A in a spherical shell at radius r with thickness dr:

$$\Omega_A(w, r) = w\,\frac{\rho_A}{m_A}\int_{E_{\rm min}(w)}^{E_{\rm max}(w)} dE_R \frac{d\sigma_A}{dE_R}(w)\,, \tag{3.2}$$

where $\rho_A(r)$ is the mass density of the element A in the Sun (ρ_A/m_A being the number density). For the numerical calculations we use the standard solar model from ref. [48]. Here, E_R is the recoil energy of the nucleus after the scattering. For a given DM velocity w there is a minimal and maximal nuclear recoil energy, $E_{\rm min}(w)$ and $E_{\rm max}(w)$, such that the DM particle gets trapped, i.e., its velocity after the scattering is less than the local escape velocity. Writing them in terms of the velocity v at infinity one has

$$E_{\rm min} = \frac{m_\chi}{2}v^2\,, \qquad E_{\rm max} = \frac{2\mu_{\chi A}^2}{m_A}(v^2 + u_{\rm esc}^2(r))\,, \tag{3.3}$$

where the former constraint is the requirement for the DM particle to be captured and the latter is based on the maximal energy transfer allowed by kinematics. In figure 1 we show $E_{\rm min}$ and $E_{\rm max}(r)$ versus velocity v for scattering on hydrogen for two different DM masses,

JCAP05(2015)036

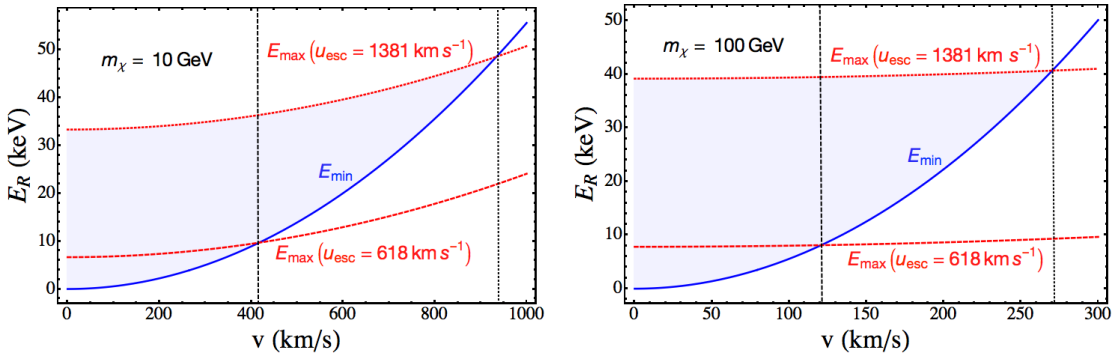

Figure 1. For hydrogen (SD), we show in blue the lower bound on the energy for DM capture in the Sun, $E_{\rm min}$, and in red the energy upper limits, $E_{\rm max}(r)$, for the two extreme escape velocities, versus the velocity v, for $m_\chi = 10\,(100)\,{\rm GeV}$, left (right). The points were they cross (indicated by the vertical dotted lines) are the maximum velocities of the DM particles, $v^p_{\rm cross}(r)$.

$m_\chi = 10$ and $100\,{\rm GeV}$, and for the two extreme values of the escape velocity in the Sun: $618\,{\rm km\,s^{-1}}$ at the surface and $1381\,{\rm km\,s^{-1}}$ in the center of the Sun. One can see that $E_{\rm min}$ and $E_{\rm max}(r)$ cross, which defines the maximum velocity the DM particles can have in order to be trapped in a single interaction, $v^A_{\rm cross}(r)$. From eq. (3.3) we find

$$v^A_{\rm cross}(r) = \frac{\sqrt{4m_A m_\chi}}{|m_\chi - m_A|} u_{\rm esc}(r) \qquad \text{or} \qquad E^A_{\rm cross}(r) = \frac{2m_A m_\chi^2}{(m_\chi - m_A)^2} u^2_{\rm esc}(r)\,. \tag{3.4}$$

Therefore, $v_{\rm cross}(r)$ decreases with DM mass m_χ, and the capture rates will decrease and eventually vanish for large DM masses. For SD interactions, where only hydrogen is relevant, we can use $m_p \ll m_\chi$ and

$$v^p_{\rm cross}(r) \approx 2\sqrt{\frac{m_p}{m_\chi}} u_{\rm esc}(r) \qquad \text{or} \qquad E^p_{\rm cross} \approx 2 m_p u_{\rm esc}(r)\,. \tag{3.5}$$

Typically, for heavier nuclei $v^A_{\rm cross}(r)$, which is relevant for SI interactions, is larger than $v^p_{\rm cross}(r)$, relevant for SD interactions.

The cross section $d\sigma_A(w)/dE_R$ in eq. (3.2) is the same as the one entering in the event rate for DD experiments. Again, restricting to contact interactions,[2] we use eq. (2.5) for SI interactions and an analogous expression for SD. For the nuclear form factors of the elements in the Sun we use the approximation $F^2_A(E_R) \simeq e^{-E_R/E_A}$, with $E_A = 3/(2m_A R_A^2)$ and $R_A = [0.91(m_A/{\rm GeV})^{1/3} + 0.3]\,{\rm fm}$ [46]. Hence, we obtain

$$C_{\rm Sun} = 4\pi\,\mathcal{C} \sum_A A^2 \int_0^{R_{\rm Sun}} dr r^2 \rho_A(r) \int_0^{v^A_{\rm cross}} dv \tilde{f}(v)\, v \int_{E_{\rm min}(v)}^{E_{\rm max}(v)} F^2_A(E_R) dE_R \tag{3.6}$$

for the capture rate in SI interactions. The coefficient $\mathcal{C}$ is defined in eq. (2.7) and contains the DM-nucleus scattering cross section. For SD interactions only hydrogen is relevant, i.e., the sum contains only one term with $A = 1$, and the form factor is trivial, $F^2_{\rm H}(E_R) = 1$.

If equilibrium between DM capture and annihilation in the Sun is reached, the final annihilation rate is independent of the annihilation cross section and is given by:

$$\Gamma_{\rm Sun} = \frac{1}{2} C_{\rm Sun}\,. \tag{3.7}$$

[2]For other types of interactions see appendix B.

JCAP05(2015)036

For equilibrum to occur, the equilibration time $t_{\rm eq}$ must be smaller than the age of the Sun, i.e., $t_{\rm eq} \ll t_{\rm Sun} \sim 4.5\,{\rm Gyr}$, where (see for instance ref. [19])

$$t_{\rm eq} = \frac{1}{\sqrt{C_{\rm Sun}\, A_{\rm Sun}}} \approx 0.5\,{\rm Gyr} \left(\frac{10^{21}\,{\rm s}^{-1}}{C_{\rm Sun}}\right)^{1/2} \left(\frac{3\cdot 10^{-26}\,{\rm cm}^3\,{\rm s}^{-1}}{\langle\sigma v\rangle}\right)^{1/2} \left(\frac{100\,{\rm GeV}}{m_\chi}\right)^{3/4} . \quad (3.8)$$

Here $A_{\rm Sun}$ is the annihilation rate in the Sun and $\langle\sigma v\rangle$ the thermal average of the annihilation cross section. As we will see in section 5 for mock data and in appendix A for DAMA, our values of the lower bound on the capture are safely above $\gtrsim 10^{21}\,{\rm s}^{-1}$ in all cases except for SI interactions in xenon, due to the small scattering cross section assumed for the mock data, $\sigma_{\rm SI} = 10^{-45}\,{\rm cm}^3\,{\rm s}^{-1}$. In this case, equilibrium may not be reached for annihilation cross sections smaller or equal than the freeze-out one. Also we note that in case of p-wave annihilations the annihilation cross section today can be much smaller than the thermal freeze-out value assumed in eq. (3.8) and depending on the capture rate equilibrium may or may not be reached.

Notice that we are neglecting evaporation, which is justified for $m_\chi \gtrsim 3\,{\rm GeV}$ [45, 46, 49]. The neutrino flux at the Earth from the annihilation channel f with branching ratio ${\rm BR}_f$ is

$$\frac{d\phi_\nu^f}{dE_\nu} = {\rm BR}_f \frac{\Gamma_{\rm Sun}}{4\pi d^2} \frac{dN_\nu^f}{dE_\nu} , \quad (3.9)$$

where d is the Sun-Earth distance and dN_ν^f/dE_ν is the neutrino spectrum per annihilation of flavour f that reaches a distance of 1 AU, which needs to take into account flavour transitions (neutrino oscillations, MSW effect), absorption and regeneration, see, e.g., refs. [50, 51].

4 Relating DM direct detection to the DM capture rate in the Sun

We now want to relate a DD signal to the DM capture rate in the Sun in a halo-independent way. We assume that the DM velocity distributions relevant in the two cases are the same. This implies two important consequences:

1. We neglect the small velocity of the Earth with respect to the Sun and adopt the approximation for $\tilde{f}$ (defined in eq. (2.4))

$$\tilde{f}_{\rm det}(v) \approx \tilde{f}_{\rm Sun}(v) \equiv \tilde{f}(v) .$$

   Hence we use that $v_e \approx 29\,{\rm km/s} \ll v_m$ for typical values of v_m. This also implies that we are ignoring the (small) annual modulation signal in the direct detection rate (we will comment on this in appendix A).

2. DM direct detection samples the DM distribution today, while for the DM capture in the Sun the velocity distribution on time scales relevant for the equilibration of capture and annihilations is relevant. We will assume that the DM velocity distribution is constant on those time scales and that the same $\tilde{f}(v)$ applies for the neutrino capture and direct detection. Similarly, we also assume that the energy density is constant on times scales relevant for equilibration and equal to the current one.

JCAP05(2015)036

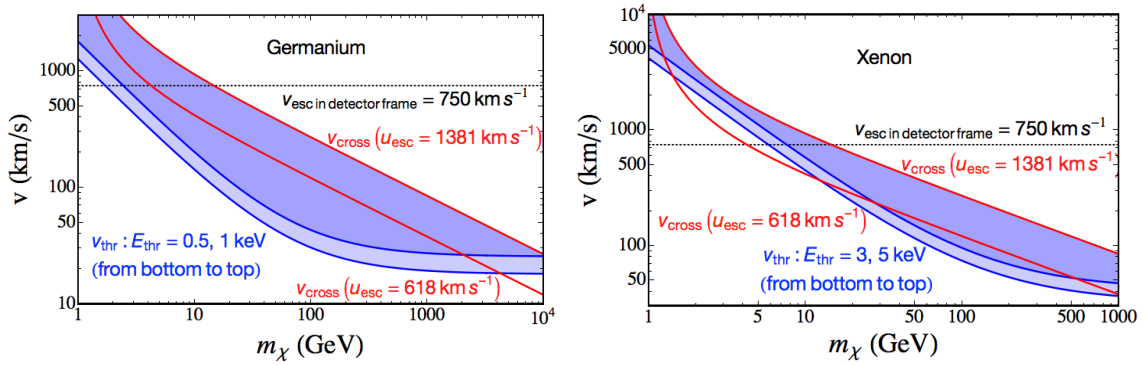

Figure 2. In blue we show the minimum velocity $v_{\rm thr}(E_{\rm thr})$ probed in a direct detection experiment versus m_χ, assuming different threshold energies $E_{\rm thr}$ and using a Ge (left) and a Xe (right) target. In red we show the maximum velocity relevant for DM capture in the Sun for scattering on hydrogen, $v^p_{\rm cross}$, for the two extreme values of $u_{\rm esc} = 1381\,{\rm km\,s^{-1}}$ in the centre of the Sun and $v_{\rm esc} = 618\,{\rm km\,s^{-1}}$ at the surface. The shaded area shows the overlap region assuming scattering in the centre of the Sun. The horizontal black line indicates approximately the galactic escape velocity in the detector rest frame.

4.1 The overlap in v_m

From inspection of the relations given in section 2 we see that direct detection is sensitive to *high* DM velocities. Let us denote the threshold energy of a given experiment by $E_{\rm thr}$. If we ignore the finite energy resolution of the experiment, this defines a threshold velocity via eq. (2.2): $v_{\rm thr} \equiv v_m(E_{\rm thr})$.[3] Hence, this experiment is sensitive to DM velocities $v > v_{\rm thr}$. In a realistic halo there will be a maximal velocity of DM particles, set by the escape velocity from the galactic gravitational potential, $v_{\rm esc}$. Since the precise value of this escape velocity is uncertain (see, e.g., ref. [52] and references therein) we want to keep the discussion as independent of this argument as possible.

In contrast to direct detection, eq. (3.6) shows that only DM velocities $v < v^A_{\rm cross}(r)$ contribute to the capture rate in the Sun. Hence, direct detection is sensitive to DM velocities above a certain value given by $v_{\rm thr}$, whereas for DM to be captured in the Sun velocities below the value set by $v^A_{\rm cross}(r)$ are relevant. In order to relate the two phenomena we need to consider the overlap regions in velocity space. If $v^A_{\rm cross} < v_{\rm thr}$, there is no overlap and direct detection and DM capture *decouple*. In this case no statement can be made halo-independently and a connection can be established only by referring to some a-priori assumptions about the DM velocity distribution.

In figure 2 we show with blue curves the minimum velocity probed in direct detection experiments versus the DM mass, using Ge (left) and Xe (right) for different examples of threshold energies. Those curves can be compared with the maximal velocity relevant for the DM capture in the Sun, $v_{\rm cross}$, which is shown with red curves for scattering on hydrogen for the two extreme values of the solar escape velocity $u_{\rm esc}$ corresponding to the values in the centre and at the surface of the Sun. From the figure we observe that for a large range of DM masses there is an overlap of the DM velocities probed by direct detection and solar capture, i.e., $v_{\rm thr} < v_{\rm cross}$, at least for scattering events which occur near the centre of the

[3] In the case of a finite energy resolution the actual threshold velocity would be somewhat smaller than the value corresponding to the nominal threshold energy of the experiment due to the reconstruction of events below the threshold at higher energies.

JCAP05(2015)036

Sun. A similar figure can be found in ref. [25], where it is also shown that $v_{\rm cross}$ is even larger for heavier nuclei relevant for SI interactions and therefore the overlap is also enhanced with respect to SD interactions.

In the following we are going to make use of the overlap region in velocity space in order to compare results from direct detection experiments to neutrino searches from the Sun without specifying any halo properties apart from the two assumptions stated at the beginning of this section. In particular, in section 4.2 below we are going to assume a positive signal in direct detection and derive a halo-independent lower bound on the capture rate in the Sun. We will use the fact that from a precise measurement of the nuclear recoil spectrum the angular averaged distribution $\tilde{f}(v)$ times the constant $\mathcal{C}$ can be extracted from the data via eq. (2.9), and we can make use of the signal precisely in the overlap region in velocity space.

Before we proceed with this, let us briefly comment on the case of a positive signal from neutrinos. In this case no direct information can be obtained about $\tilde{f}(v)$, and the signal can come from any DM velocity below $v_{\rm cross}$. For a positive neutrino signal no general lower bound for the direct detection rate can be established halo-independently, since the capture may happen entirely from velocities below the threshold of the DD experiment. If no signal is seen in direct detection at the relevant level, such a situation could point to a halo dominated by low velocity DM particles (in the solar frame), for instance a co-rotating dark disk [22]. Alternatively this may indicate more exotic particle physics such as self-interacting DM, which enhances the capture rate by DM-DM scattering, independently of the DM-nucleus scattering cross section [53]. Another example of a modified relation between the DD signal and capture in the Sun is inelastic DM scattering [54–56]. These cases will be studied in a future work.

4.2 A lower bound on the capture rate from a positive direct detection signal

We can derive a lower bound on the capture rate, eq. (3.6), by using that for any positive function $H(v) \geq 0$ we have that $\int_0^{v^A_{\rm cross}} H(v)\, dv \geq \int_{v_{\rm thr}}^{v^A_{\rm cross}} H(v)\, dv$ for $v_{\rm cross} \geq v_{\rm thr}$. Therefore we have

$$C_{\rm Sun} \geq 4\pi \sum_A A^2 \mathcal{C} \int_0^{R_{\rm Sun}} dr r^2 \rho_A(r) \int_{v_{\rm thr}}^{v^A_{\rm cross}} dv\, \tilde{f}(v)\, v\, \mathcal{F}_A(v,r), \tag{4.1}$$

where we defined

$$\mathcal{F}_A(v,r) \equiv \int_{E_{\rm min}(v)}^{E_{\rm max}(v)} F_A^2(E_R) dE_R\,, \tag{4.2}$$

with $E_{\rm min}(v)$ and $E_{\rm max}(v)$ given by eq. (3.3). Notice that $E_{\rm max}(v)$, $\mathcal{F}_A(v,r)$ and $v^A_{\rm cross}$, eq. (3.4), depend on r via $u_{\rm esc}(r)$.

Let us assume now that a significant direct detection signal has been observed. We can then use eq. (2.9) to obtain $\tilde{f}(v)$ from the data and insert it in eq. (4.1):

$$\begin{aligned} C_{\rm Sun} &\geq 4\pi \sum_A A^2 \int_0^{R_{\rm Sun}} dr r^2 \rho_A(r) \int_{v_{\rm thr}}^{v^A_{\rm cross}} dv \left(-\frac{d\tilde{\eta}(v)}{dv}\right) \mathcal{F}_A(v,r) \\ &= 4\pi \sum_A A^2 \int_0^{R_{\rm Sun}} dr r^2 \rho_A(r) \left[\tilde{\eta}(v_{\rm thr}) \mathcal{F}_A(v_{\rm thr},r) + \int_{v_{\rm thr}}^{v^A_{\rm cross}} dv\, \tilde{\eta}(v)\, \mathcal{F}'_A(v,r)\right], \end{aligned} \tag{4.3}$$

JCAP05(2015)036

where in the last line we integrated by parts, with $\mathcal{F}_A(v^A_{\rm cross}, r) = 0$ and $\mathcal{F}'_A(v,r) \equiv d\mathcal{F}_A(v,r)/dv$. For SD interactions only hydrogen is relevant and we have $F_{\rm H}(E_R) = 1$, and

$$\mathcal{F}_{\rm H}(v,r) = E_{\rm max}(v,r) - E_{\rm min}(v)\,, \qquad \mathcal{F}'_{\rm H}(v,r) = \left(\frac{4\mu_A^2}{m_A} - m_\chi\right) v \leq 0\,. \tag{4.4}$$

The direct detection signal has to be precise enough for $\tilde{\eta}(v)$ to be extracted from the observed energy spectrum via eq. (2.9) with sufficient precision. Either the derivative or the function $\tilde{\eta}(v)$, including its value at the experimental threshold, have to be determined, including unfolding of experimental resolutions and backgrounds. This will require a significant number of events such that an accurate spectral analysis can be performed. If those conditions are met, eq. (4.3) provides a lower bound on the capture rate in the Sun without specifying the DM velocity distribution, the galactic escape velocity, the scattering cross section or the local DM density. This lower bound is the central result of this paper and we will illustrate it numerically in the following section for possible future signals in DD experiments.

5 Numerical examples

5.1 Mock data for direct detection

The halo-independent bound on the DM capture rate in the Sun derived in the previous section will be useful once a clear and highly significant signal in a direct detection experiment has been observed.[4] In the following we will assume that the DM-nucleon scattering cross section is just below the current limits [5, 8], which will allow upcoming experiments to obtain a significant signal. As representative examples we will consider a future xenon based experiment [57–59] as well as a germanium detector [60, 61]. For calculating mock data we adopt the conventional Maxwellian velocity distribution (SHM) with $\bar{v} = 220$ km/s, truncated at the escape velocity of $v_{\rm esc} = 544$ km/s, and we assume a local DM density $\rho_\chi = 0.3\,{\rm GeV/cm^3}$. The velocity of the Sun in galactic coordinates is (10, 233, 7) km/s.

For the xenon experiment we adopt a threshold of 5 keV (we also show the effect of a reduced threshold of 3 keV below) and we take natural abundances of the isotopes with spin, ^{129}Xe (26.4 %) and ^{131}Xe (21.2 %). We use the values of $10^{-45}\,{\rm cm^2}$ for the SI cross section and $2 \cdot 10^{-40}\,{\rm cm^2}$ for the SD cross section, with equal couplings to protons and neutrons in both cases. Assuming $m_\chi = 100\,{\rm GeV}$, for an exposure of 1 ton yr at 100% efficiency about 154 (267) events would be observed in the energy range 5–45 keV for SI (SD) case.

We also generate mock data for a future germanium experiment, with a threshold of 1 keV, focusing on low DM masses. Assuming a DM mass $m_\chi = 6\,{\rm GeV}$ and cross sections of $\sigma_{\rm SI} = 5 \cdot 10^{-42}\,{\rm cm^2}$ and $\sigma_{\rm SD} = 2 \cdot 10^{-40}\,{\rm cm^2}$ (with equal couplings to protons and neutrons) we would obtain about 1.5×10^4 (2–3) events for SI (SD) interactions in the energy range 1–10 keV for an exposure of 100 kg yr with energy resolution of 30%. While the SI case will allow for a high statistics reconstruction of the event spectrum, this will not be possible for

[4] The CDMS collaboration reports 3 candidate events from their data with a silicon target, with a 0.19% probability for the known-background-only hypothesis when tested against the alternative DM+background hypothesis [7]. In order to apply our bounds a detailed spectral measurement is required and not enough information can be extracted from the 3 observed events in CDMS-Si. However, motivated by this potential signal, we take DM parameter values similar to those preferred by CDMS-Si events for our example of mock data in germanium. The annual modulation signal reported by the DAMA/LIBRA collaboration [1] will be discuss in appendix A. We emphasize that both signals are either excluded or in strong tension with several other experiments [2–6, 8] (see for instance refs. [35, 42] for halo-independent analyses).

JCAP05(2015)036

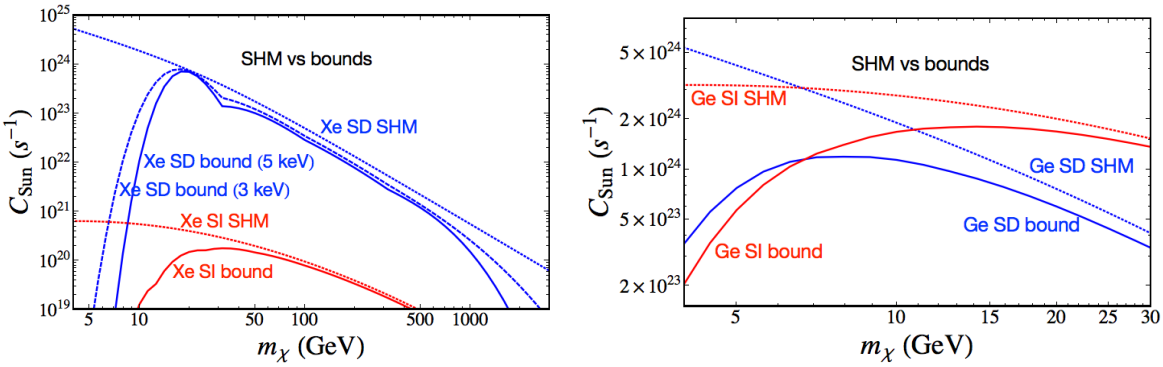

Figure 3. Lower bounds on the DM capture rate in the Sun for xenon (left) and germanium (right) DD mock data as described in the text, both for SI (red curves) and SD (blue curves) interactions. For illustrative purposes, in the Xe SD case we show the effect of changing the default threshold energy of $E_{\rm thr} = 5\,\text{keV}$ (solid) to 3 keV (dashed). The dotted curves correspond to the actual capture rate. To calculate the DD mock data as well as the capture rate we assume the standard halo model.

the SD case with the assumed parameters. This follows from the missing A^2 enhancement with respect to SI interactions, as well as the small abundance of only 7% of the relevant Ge isotope with spin. Nevertheless we are going to include SD interactions in the following discussion, keeping always in mind that this will require larger exposures or a different target nucleus with better sensitivity to SD interactions. In addition, the bounds are stronger for larger DM masses, but we want to provide an illustrative example for the small mass region.

In the following analysis we neglect the energy resolution, effects of binning the data, possible contamination with background, experimental errors, and nuclear form factor uncertainties (we comment on form factors later in subsection 5.4). Hence, we assume that $\tilde{\eta}(v_m)$ can be extracted from the observed nuclear recoil spectrum (for a specified m_χ). This idealized analysis suffices to illustrate the power of our bounds. Once applied to real data an appropriate statistical analysis will have to be performed.

In figure 3 we show the lower bound on the capture rate for the mock data of future DD xenon (left) and germanium (right) experiments as described above, both for SD and SI interactions and compare them to the true capture rate assuming the SHM. In the case of Ge we focus on the low DM mass region, i.e., $m_\chi \lesssim 30\,\text{GeV}$, keeping in mind that the bounds are stronger (i.e., closer to the true capture rate) for $m_\chi \gtrsim 20\,\text{GeV}$. The bounds as well as the capture rate are shown for the "true" DM mass, which has been used to calculate the mock data. We see that our bounds are strong in a large portion of parameter space for the xenon experiment: $20 \lesssim m_\chi \lesssim 1000\,\text{GeV}$ for SD, and for $m_\chi \gtrsim 50\,\text{GeV}$ for SI.

5.2 Limits from neutrino telescopes

In order to compare the lower limit on the DM capture rate in the Sun from a DM direct detection signal with the upper bounds on the neutrino rate from neutrino telescopes we proceed as follows. We assume equilibrium between capture and annihilations and the neutrino-induced muon rate in neutrino telescopes will then depend on the specific annihilation channel, which depends on the particle physics model for DM. In particular cases, the high-energy neutrino rate may be strongly suppressed by the available annihilation channels, for instance for annihilations into $e^\pm, \mu^\pm$ or u, d, s quarks (see, however, ref. [62] for higher

JCAP05(2015)036

order effects). Hence, translating a given upper bound on the neutrino-induced muon rate into a bound on the capture rate depends on the DM annihilation channel, see section 3.

Below we are going to compare the lower bounds on $C_{\rm Sun}$ to the limits from IceCube (IC) and Super-Kamiokande (SK). For IC we use the upper bounds of ref. [11], where results are given directly as upper limit on the capture rate for various annihilation channels as a function of the DM mass. We will show results for two cases, namely annihilations into $bb+\tau\tau$ and into $WW+\tau\tau$ (we keep particle/antiparticle notation implicit for annihilation products). For SK there are no limits on the capture rate available. Therefore, for annihilation channels into bb and $\tau\tau$ in the low DM mass region (up to 200 GeV) we extract the upper limits on the capture from the upper limits on the scattering cross section given by the most recent SK results [13]. For the large mass region in these channels, and also for direct annihilation into neutrinos ($\nu_\mu\nu_\mu$), we use the limits on the capture rate calculated in ref. [63] (table II) based on SK data from ref. [10]. The quoted bounds at the 90% CL from IC and SK apply assuming that annihilations proceed with 100% branching ratio into the indicated channels.

5.3 Comparison of direct detection and neutrino data

In order to apply the lower bound on the capture rate derived in section 4.2 one has to specify the DM mass and the couplings to neutrons and protons. For the moment we will restrict the analysis to equal couplings to neutrons and protons, and we will come back to this point in section 5.4. Regarding the DM mass, in general it cannot be extracted from a DD signal without referring to a specific DM halo model. Therefore, we do the analysis without assuming that the DM mass is known. We calculate mock data for a fixed "true" DM mass, but then we apply the lower bound on $C_{\rm Sun}$ as a function of m_χ (different from the "true" value). This procedure resembles the situation we would face in case of applying the method to real data. If the mass was known from some other data (e.g., an observation at LHC or a γ line signal from indirect DM searches) one would of course perform the analysis only for that DM mass.

In figure 4 we show the lower bounds on the capture, assuming a true (but unknown) dark matter mass of $m_\chi = 30\,\text{GeV}$ (upper panels), 100 GeV (middle panels), and 300 GeV (lower panels) for a xenon DD experiment and compare them to the limits from IC and SK. While for SI interactions the lower bound from DD would be consistent with the limits from IC and SK, we see that for SD interactions tension arises if DM annihilates into neutrinos or into $\tau\tau/WW$. In the right panels we show the ratio of the upper limit on $C_{\rm Sun}$ to the lower bound. This can be interpreted as an upper bound on the branching ratio of the corresponding annihilation channel. This is conservative, since it assumes that there are no neutrinos from any other annihilation channels, which typically will not be the case.

We see that direct annihilations into neutrinos would be constrained to branching ratios at the few % level, with some dependence on the DM mass. Annihilations into $\tau\tau, WW$ could be constrained at the 10% level. However, note that for true $m_\chi \lesssim 100\,\text{GeV}$ the bound is stronger when applied at a "wrong" DM mass, i.e., for values of m_χ which are larger than the actual true value. When using the correct value of m_χ the limits for the assumptions adopted here would be rather weak.

In figure 5 we show the lower bounds on the capture (left) and the upper bounds on the branching ratios for different channels (right), assuming the low threshold germanium experiment. Since this configuration is most sensitive at low DM masses we take here a "true" DM mass of 6 GeV. In this case SD and SI interactions lead to similar lower bounds which potentially can constrain annihilations into channels leading to neutrinos. Again we

JCAP05(2015)036

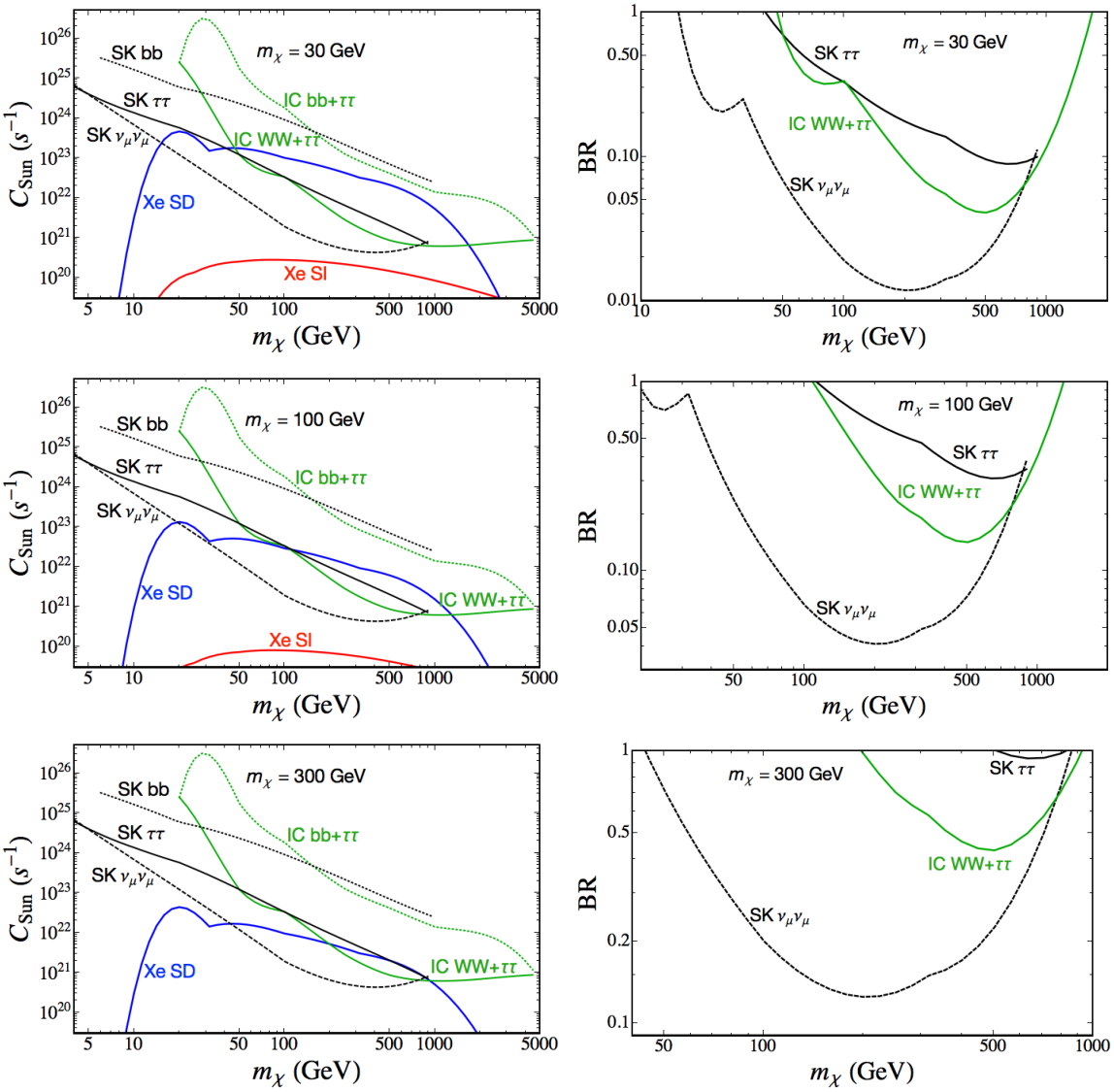

Figure 4. Left: lower bounds on the capture rate from a future xenon DD experiment for SI (red) and SD (blue) interactions compared to the 90% CL upper limits for the combined annihilation channels $WW, \tau\tau$ and $bb, \tau\tau$ from IceCube (IC, green curves) [11] and the channels $\nu_\mu\nu_\mu$, $\tau\tau$, bb from Super-Kamiokande (SK, black curves) [10, 13, 63]. Right: upper bounds on the branching ratios versus dark matter mass for SD interactions. To calculate the DD mock data we assume a "true value" for the DM mass of $m_\chi = 30, 100, 300\,\text{GeV}$ in the top, middle, bottom panels, respectively, and values of $10^{-45}\,\text{cm}^2$ for the SI cross section and $2 \cdot 10^{-40}\,\text{cm}^2$ for the SD cross section, with equal couplings to protons and neutrons in both cases. Assumptions about the mock data for the DD experiment are given in section 5.1.

note the feature that bounds get stronger when applied for the "wrong" DM mass, in which annihilations into $\tau\tau$ become also constraining.

We note that our comparison of DD and neutrino data is not fully consistent, in the sense that we are comparing a possible signal in a future DD experiment with current limits from neutrino telescopes. When the potential signals from DD will be available, limits from IC and/or SK may have improved and upgraded and/or new neutrino telescopes may be in

JCAP05(2015)036

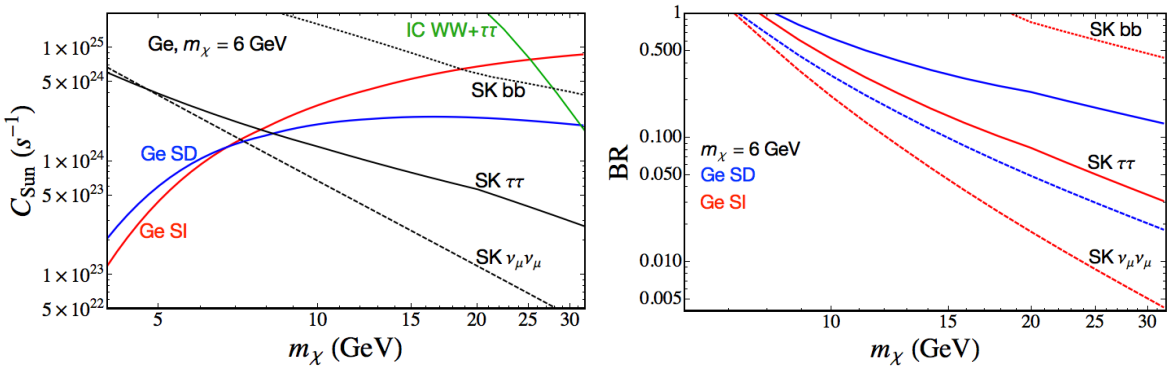

Figure 5. Left: lower bounds on the capture rate from a future germanium DD experiment for SI (red) and SD (blue) interactions compared to the 90% CL upper limits for the combined annihilation channels $WW, \tau\tau$ from IceCube (IC, green curves) [11] and the channels $\nu_\mu\nu_\mu$, $\tau\tau$, bb from Super-Kamiokande (SK, black curves) [10, 13, 63]. Right: upper bounds on the branching ratios versus dark matter mass. To calculate the DD mock data we assume a "true value" for the DM mass of $m_\chi = 6\,\text{GeV}$ and cross sections of $\sigma_{\rm SI} = 5 \cdot 10^{-42}\,\text{cm}^2$ and $\sigma_{\rm SD} = 2 \cdot 10^{-40}\,\text{cm}^2$ (equal couplings to protons and neutrons). Assumptions about the mock data for the DD experiment are given in section 5.1.

place [64–66]. In this sense our results are conservative, since the comparison may become more stringent than what is shown here.

Let us comment briefly on the annual modulation of the DD signal. We expect that using information on the modulation in addition to the unmodulated rate does not provide significantly stronger bounds on the capture rate. If a future experiment only measures the modulation amplitude but cannot distinguish the unmodulated DM rate from background (similar to the DAMA experiment [1]) one can use the results of refs. [34, 35] to derive a lower bound on $C_{\rm Sum}$ based on the modulation amplitude. Those bounds require some additional (modest) assumptions on the halo and they can be found in appendix A, where we also apply those bounds for the DAMA signal [1], which however is incompatible with other DD limits halo-independently [35].

5.4 Uncertainties due to form factors and unknown couplings to protons and neutrons

In this section we discuss the uncertainties associated to nuclear form factors, as well as the case of arbitrary couplings to neutrons and protons. Different calculations of form factors sometimes lead to large differences, especially for SD interactions and heavy nuclei such as xenon, see for instance refs. [67–71] for discussions. In our numerical calculations based on mock data no form factor appears, since we assume that the "correct" one is used, when extracting the velocity distribution from the observed rate via eq. (2.9). If a "wrong" form factor was used in eq. (2.9) it would modify the extracted velocity distribution, $\tilde{f}_{\rm extr}(v)$, in the following way:

$$\mathcal{C}\tilde{f}_{\rm extr}(v) = \mathcal{C}\tilde{f}(v)\frac{F^2_{\rm true}(E_R)}{F^2_{\rm wrong}(E_R)} - \frac{\tilde{\eta}(v)}{v}\frac{d}{dv}\left(\frac{F^2_{\rm true}(E_R)}{F^2_{\rm wrong}(E_R)}\right). \tag{5.1}$$

Let us focus on the case of SD interactions (where form factor uncertainties can be large) and consider also general couplings to neutrons (a_n) and protons (a_p). In this case the form

JCAP05(2015)036

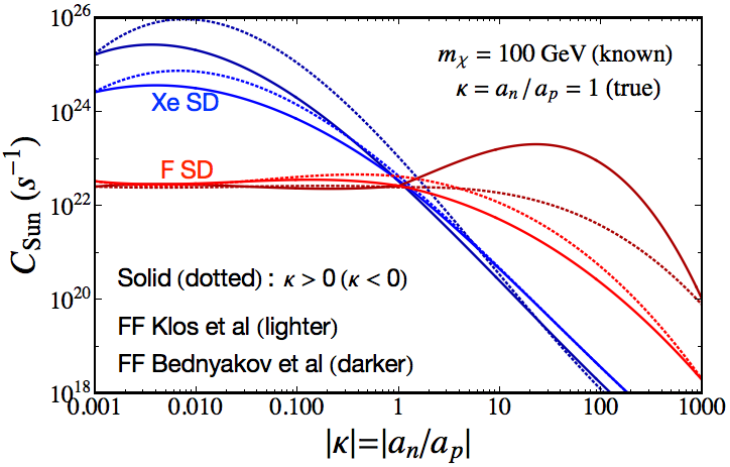

Figure 6. Lower bound on the capture rate for SD interactions from mock data from experiments using xenon (red) and fluorine (blue). Mock data is generated for a DM mass of $m_\chi = 100\,\text{GeV}$, $\sigma_\chi^p = 2 \cdot 10^{-40}\,\text{cm}^2$, and equal couplings to protons and neutrons ($\kappa = a_n/a_p = 1$). The lower bound on $C_{\rm Sun}$ is shown as a function of $|\kappa|$ (i.e., using a "wrong" value of κ when using the mock data to calculate the bound), where the solid (dotted) curves correspond to $\kappa > 0$ ($\kappa < 0$). Dark (light) colours correspond to the form factors from ref. [67] (ref. [70]).

factor can be expressed in terms of the structure functions $S_{ij}(E_R)$ as

$$F_{\rm SD}^2(E_R) = \left(1+\kappa\right)^2 S_{00}(E_R) + \left(1-\kappa^2\right) S_{01}(E_R) + \left(1-\kappa\right)^2 S_{11}(E_R)\,, \tag{5.2}$$

where we define $\kappa \equiv a_n/a_p$ and we have absorbed a_p in the cross section σ_χ^p. Now we can use this relation together with eq. (5.1) to test both the impact of using a "wrong" form factor as well as "wrong" values of κ when deriving the bound on the capture rate from mock data.

In order to illustrate those effects we generate mock data assuming SD interactions for a neutron-dominated experiment (xenon) and for a proton-dominated one (fluorine). We use the same parameters for the mock data as in section 5.1 for both experiments, with $\sigma_{\rm SD} = 2 \cdot 10^{-40}\,\text{cm}^2$, a DM mass of $m_\chi = 100\,\text{GeV}$, and $E_{\rm thr} = 3\,\text{keV}$. For these parameter values, we predict 78 events in the energy range $[3, 10]\,\text{keV}$ for a fluorine experiment with total exposure of $100\,\text{kg}\cdot\text{y}$. To generate mock data we assume equal couplings to protons and neutrons ($\kappa = 1$).

In figure 6 we show the lower bound on the capture rate as a function of κ, illustrating the case of using a "wrong" ratio of neutron to proton couplings when analysing the data. For $\kappa \sim 1$ both F and Xe give similar lower bounds, with the difference coming from their minimum velocities at the threshold ($v_{\rm thr}$) due to their different masses. For the xenon experiment, for $|\kappa| \gg 1$, the capture rate vanishes, since in xenon spin is mostly carried by the neutron. Hence, for $|\kappa| \gg 1$ the DD signal is dominated completely by neutrons and since the capture in the Sun is set by protons, $C_{\rm Sun}$ becomes suppressed by $1/\kappa^2$ in that case. On the other hand, the spin of the fluorine nucleus is mainly provided by a proton. Hence, for $|\kappa| < 1$ the bound on the capture rate becomes independent of the ratio of the couplings, since both DD and $C_{\rm Sun}$ are controlled by interactions with protons.

We also illustrate the effect of using different form factors in figure 6, comparing form factor calculations from ref. [67] (darker colours) and ref. [70] (lighter colours). We see that those two examples give similar results in the regime where the interaction is "large", i.e.,

JCAP05(2015)036

for neutron (proton) dominated interactions for xenon (fluorine). However, in the opposite case those two form factor calculations lead to very different results. For $|\kappa| < 1$ (proton domination), a xenon experiment would give very strong bounds on the capture rate, since interactions are suppressed for DD, and explaining the assumed signal would require a very large scattering cross section. However, in this regime the bounds differ by about one order of magnitude between the two form factor models. Similarly, for $|\kappa| > 1$ (neutron domination), the bound on the capture rate from a fluorine experiment changes by more than a factor 100 between the two form factor calculations.

Let us stress an important point related to using "wrong" values of κ. This discussion is mostly relevant if data is available only from one experiment (or experiments with the same spin structure). If a significant signal from xenon as well as fluorine is observed (such as assumed in our mock data), then the neutron to proton ratio κ is essentially determined by the relative strength of the two signals. This emphasizes the need of data from complementary targets. A similar discussion will also apply for SI interactions with arbitrary couplings to neutrons and protons. We leave a detailed study of SI interactions with general isospin structure for future work.

In figure 6 we have changed the form factors both for generating mock data as well as calculating the bound on the capture rate, i.e., we have always used the "correct" form factor. We have also tested the impact of adopting a "wrong" form factor by using eq. (5.1). By comparing the form factors from refs. [67] and [70] in this way we find in some cases even unphysical negative values for $\tilde{f}_{\rm extr}(v)$. This means that the wrong form factor leads to inconsistent results and one would be able to see from the observed spectrum that data are not consistent with that particular form factor choice. Hence, we note that form factor uncertainties are important, but once a precise spectrum from DD is available (such as necessary for our method to work) we will have an additional tool at hand to test different form factor models.

6 Discussion and conclusions

We have established a halo-independent framework to relate a signal in a DM direct detection experiment to the neutrino rate in neutrino telescopes from DM annihilations in the Sun. Assuming that the DM velocity distribution and the DM density are constant on time scales relevant for equilibration in the Sun, we have derived a lower bound for the DM capture rate in the Sun in terms of a positive signal in a direct detection experiment, see eq. (4.3). If DM capture and annihilation in the Sun are in equilibrium we obtain (conservative) upper bounds on branching fractions for annihilations in channels involving neutrinos from the comparison of the lower bound on the capture rate from a direct detection signal with the upper limits from neutrino telescopes.

The lower bounds are based on the part in DM velocity space which contributes to both the capture in the Sun as well as the scattering in direct detection experiments. We find that for typical threshold energies of direct detection experiments a significant overlap region exists to apply our bounds. Hence, the lower bounds are independent of the velocity distribution, the escape velocity, the cross section or the local DM density, although we implicitly assume that these values are such that a direct detection signal can be measured. With some additional modest assumptions on the halo properties the bound can also be used for an annual modulation signal, as explained in appendix A.

JCAP05(2015)036

To illustrate the power of the bounds, we have applied them to mock data from future xenon and germanium experiments, assuming that the true DM cross section is not too far from the current upper bounds. In such a case the halo-independent comparison to present limits from Super-Kamiokande and IceCube leads to non-trivial bounds on the branching fraction for direct annihilations into neutrinos, if the scattering is spin-dependent. In some cases also annihilations into $\tau\tau$ start getting constrained. For spin-independent interactions current constraints are weak. In general we note that bounds are stronger for DM masses in the range between 100 to 500 GeV. For lower DM masses the lower bound from direct detection as well as the limits from neutrino telescopes become weaker. Those results can be found in figures 4 and 5. We note that this method is expected to become more powerful when data from future neutrino telescopes such as IceCube-Pingu, Hyper-Kamiokande, or KM3NET become available.

The halo-independent comparison has to be done for a specific model for the DM-nucleon interaction (and as a function of the DM mass). In our work we mostly assumed either SI or SD elastic scattering with equal couplings to neutrons and protons. Generalization to other types of couplings is straightforward. As an example we discussed in section 5.4 the case of SD interactions with arbitrary couplings to neutrons and protons. This leads to interesting situations, since only scattering on free protons is relevant for the capture in the Sun, whereas for direct detection the sensitivity is governed by the spin-composition of the target nucleus. One may imagine a situation where the spin of the nucleus is dominated by neutrons, in which case the neutrino and direct detection signals largely decouple. In order to exclude such a case it will be essential that data from target nuclei with spin carried by protons is available. Another case in which a DD signal does not always imply a neutrino signal from the Sun is asymmetric DM (see ref. [72] for a recent review). While our bounds on the capture rate would still apply, in those models annihilations are often suppressed due to the lack of anti-DM, and therefore a possible signal from neutrinos becomes very model dependent.

In our work we always assumed that the differential scattering cross section $d\sigma/dE_R$ is proportional to $1/v^2$, which is true for DM-nucleon contact interactions, but in general this may not be the case for more exotic types of interactions (see for instance ref. [37] for generalizing halo-independent methods for direct detection to such cases). In appendix B we show that it is straightforward to generalize our lower bound on the capture rate to all cases where the velocity and nuclear recoil energy dependence of the differential cross section factorizes as $d\sigma/dE_R = g(v)h(E_R)$. Considering more complicated models is beyond the scope of this paper and is left for future work. Another particle physics variation for which our results do not apply directly is inelastic scattering of the type $\chi + N \to \chi^* + N$, where the mass difference between χ and χ^* is of the order of the DM kinetic energy. This will change the kinematics of the scattering and generically for $m_{\chi^*} > m_\chi$ the capture rate is increased [54–56], see ref. [38] for halo-independent considerations in the context of DD. We leave also the generalization of the lower bound on the capture rate to this case for future work.

To conclude, we would like to emphasize that in the presence of a DD signal and a signal of neutrinos from the Sun, before proceeding to extract the parameters by doing a fit to both, one should first check if the lower bounds on the capture derived here are fulfilled for some combination of annihilation channels and branching ratios. This would provide a halo-independent consistency check for both signals.

JCAP05(2015)036

Acknowledgments

We thank Joakim Edsjö for useful discussions. This work was supported by the Göran Gustafsson Foundation [M.B.]. We also thank the Nordita Scientific Program "News in Neutrino Physics", where this work was initiated.

A Lower bound on the capture for annual modulation signals

The change of the velocity of the detector relative to the DM halo due to the Earth's rotation around the Sun leads to an annual modulation of the event rate in a DD experiment [29, 30]. We denote the amplitude of the modulation expressed in v_m space by $A_\eta(v_m)$. Information from a modulation signal can be combined with the halo-independent lower bound on the capture rate, eq. (4.3), by using halo-independent upper bounds on the annual modulation in terms of the average rate $\overline{\eta}(v_m)$ derived in ref. [34] and applied in refs. [35, 38]. Those bounds are based on an expansion in the Earth velocity v_e, using that v_e/v is small for $v \geq v_m$ for typical values of v_m relevant for experiments. In such an expansion the time independent rate appears at zeroth order, whereas the annual modulation amplitude is of linear order in v_e.

If we assume that the DM velocity distribution is constant on time scales of years and constant in space on scales of the Sun-Earth distance, one can derive the bound [34]

$$A_\eta(v_m) \leq v_e \left[-\frac{d\overline{\eta}}{dv_m} + \frac{\overline{\eta}(v_m)}{v_m} - \int_{v_m} dv \frac{\overline{\eta}(v)}{v^2} \right] . \tag{A.1}$$

Note however, that the lower bounds on the capture rate in eq. (4.3) require a lower bound either on $(-d\overline{\eta}/dv_m)$ or on $\overline{\eta}(v_m)$, which cannot be obtained in terms of $A_\eta(v_m)$ alone from eq. (A.1). In principle eq. (A.1) can be re-written as a lower bound on $(-d\overline{\eta}/dv_m)$ involving both, $A_\eta(v_m)$ and $\overline{\eta}(v_m)$. Hence, this would require an experiment able to determine the modulation amplitude as well as the unmodulated rate. Moreover we do not expect a significant stronger lower bound on $C_{\rm Sun}$ from such a procedure for modulation amplitudes which fulfill eq. (A.1) (as they must to be consistent with a DM signal).

Adopting some modest additional assumptions on the halo another bound on the modulation amplitude can be derived. If there is only one preferred direction in the DM velocity distribution one finds (see ref. [34] for details):

$$A_\eta(v_m) \leq -v_e \sin\alpha_{\rm halo} \frac{d\overline{\eta}}{dv_m}, \tag{A.2}$$

where α is the angle between the preferred DM direction and the direction perpendicular to the Earth's orbit. Assuming an observed signal for $A_\eta(v_m)$, this provides us with a lower bound on $(-d\overline{\eta}/dv_m)$, which can be directly plugged in eq. (4.3) and we get:

$$C_{\rm Sun} \geq 4\pi \sum_A A^2 \int_0^{R_{\rm Sun}} dr r^2 \rho_A(r) \int_{v_{\rm thr}}^{v^A_{\rm cross}} dv \, \frac{\tilde{A}_\eta(v)}{\sin\alpha_{\rm halo}\, v_e} \mathcal{F}_A(v), \tag{A.3}$$

where in the last line we used $\tilde{A}_\eta(v) \equiv \mathcal{C}\, A_\eta(v)$. In the following we will adopt the most conservative option $\sin\alpha_{\rm halo} \simeq 1$, but notice that in cases where the preferred DM direction is set by the direction of the Sun relative to the DM halo (e.g., for a halo with a dark disk) one has $\sin\alpha_{\rm halo} \simeq 0.5$ and the bounds scale accordingly.

JCAP05(2015)036

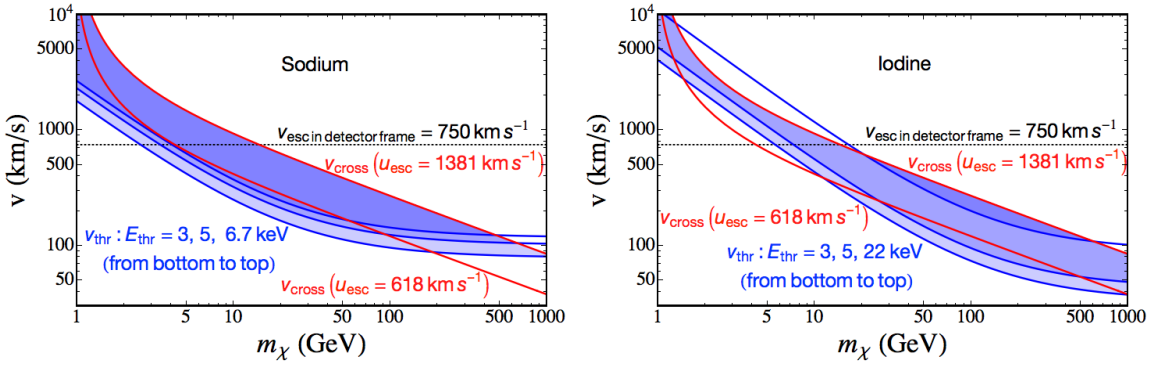

Figure 7. In blue we show the minimum velocity $v_{\rm thr}(E_{\rm thr})$ probed in a direct detection experiment versus m_χ, assuming different threshold energies $E_{\rm thr}$ and using a Na (left) and a I (right) target. In red we show the maximum velocity relevant for DM capture in the Sun, $v^p_{\rm cross}$ for scattering on hydrogen for the two extreme values of $u_{\rm esc} = 1381\,{\rm km\,s^{-1}}$ in the centre of the Sun and $v_{\rm esc} = 618\,{\rm km\,s^{-1}}$ at the surface. The shaded area shows the overlap region assuming scattering in the centre of the Sun. The horizontal black line indicates approximately the galactic escape velocity in the detector rest frame.

Notice that observing annual modulation with typical exposures (and allowed cross section values) is extremely hard (see for instance ref. [73]). The DAMA/LIBRA experiment reports an annual modulation of the signal in their NaI scintillator detector, with a period of one year and a maximum around June 2nd with very high statistical significance [1]. This modulation is strongly disfavoured by other experiments halo-independently, both for elastic SI and SD interactions [35] and for inelastic scattering [38]. Despite these problems of the DM interpretation of the DAMA modulation signal we will use it in the following to illustrate the lower bounds on the capture rate eq. (A.3) based on a modulation signal.

A.1 The DAMA modulation signal

In figure 7 we show the overlap in v_m space between DAMA and the DM capture in the Sun assuming scattering either on Na or on I. Na dominates for DM masses $m_\chi \lesssim 20\,{\rm GeV}$, whereas iodine is relevant for larger DM masses. For sodium we observe a large overlap region. Note that the DAMA threshold of 2 keVee corresponds to a recoil threshold of 6.7 keV (Na) and 22 keV (I) for usual quenching factors. This implies a relatively small overlap region in the case of iodine, especially for the SD case shown in figure 7.

To obtain a lower bound on the capture rate from DAMA data we consider a binned version of eq. (A.3) and use the observed values of $\tilde{A}_\eta(v_m)$ corresponding to the energy bins reported by DAMA, see refs. [34, 35, 38] for details on this procedure. We assume either elastic SI or SD scattering on Na or on I with equal couplings to protons and neutrons. The resulting lower bounds on the capture rate are shown in figure 8 both for SI and SD, together with the 90% CL upper limits on the capture from neutrino telescopes.

From the left panel we see that for scattering on sodium there is tension between the lower and upper bounds implying that for SI DM annihilation into neutrinos and $\tau\tau$ (bb) are strongly constrained for $m_\chi \gtrsim 5\,{\rm GeV}$ (15 GeV), while SD is excluded for all channels.

For scattering on iodine shown in the right panel of figure 8 we note the strong dependence on the DM mass for SD scattering. This can be understood from figure 7, which shows that only for a small range of DM masses there is overlap in v_m space. For SI interactions $v_{\rm cross}$ is larger (not shown in the plot), leading to larger overlap in v_m space, and we ob-

JCAP05(2015)036

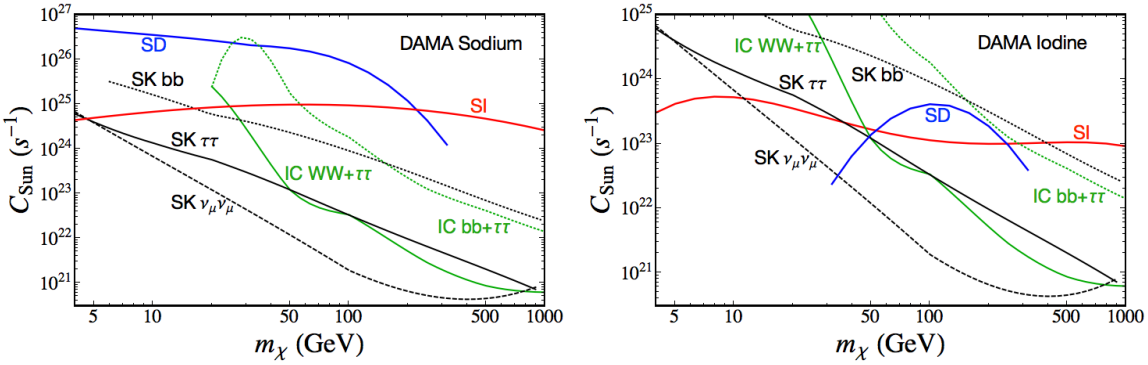

Figure 8. Lower bound on the capture rate from DAMA data assuming scattering on sodium (left) or iodine (right) for SI (red) and SD (blue) interactions, using the bound from eq. (A.3). Also shown are the 90% CL upper bounds from IceCube [11] for annihilations into $WW+\tau\tau$ and $WW+bb$ (green curves), and from Super-Kamiokande into bb, $\tau\tau$, and $\nu_\mu\nu_\mu$ [10, 13, 63] (black curves).

serve strong bounds on the annihilations shown in figure 8 for $m_\chi \gtrsim 35\,\text{GeV}$ (and even for $m_\chi \gtrsim 10\,\text{GeV}$ for the neutrino channel).

B Beyond contact interactions

In the main text of the paper we have always assumed contact interactions between DM and the nucleus, which leads to a $1/v^2$ dependence of the differential scattering cross section. In more exotic models also other dependences on v and/or E_R are possible, see for instance refs. [21, 37, 63] in the context of DD and the neutrino signal. Our bounds can be generalized in a straightforward way if the dependence of v and E_R factorizes. Let us assume that the differential cross section on the nucleus with mass number A can be written in the form

$$\frac{d\sigma_A}{dE_R} = g_A(v) h_A(E_R)\,. \tag{B.1}$$

In the conventional case considered in the main text we have $g_A(v) \propto 1/v^2$ and $h_A(E_R) = F_A^2(E_R)$, see eq. (2.5).

From the measured recoil spectrum in a DD experiment, $\mathcal{R}(E_R)$, we can then extract the DM velocity distribution by

$$\tilde{f}(v)\, v = -\frac{m_\chi m_A}{\rho_\chi v^2 g_A(v)} \frac{d}{dv}\left(\frac{\mathcal{R}(E_R)}{h_A(E_R)}\right)\,. \tag{B.2}$$

Using this in the expression for the capture rate in the Sun (eqs. (3.1) and (3.2)) we find that the bound eq. (4.3) becomes

$$C_\text{Sun} \geq 4\pi \sum_A \int_0^{R_\text{Sun}} dr r^2 \rho_A(r) \int_{v_\text{thr}}^{v^A_\text{cross}} dv \left[-\frac{d}{dv}\left(\frac{\mathcal{R}(E_R)}{h_{A_\text{DD}}(E_R)}\right)\right] \frac{w^2 g_A(w)}{v^2 g_{A_\text{DD}}(v)} \mathcal{H}_A(E_R, r) \tag{B.3}$$

where A_DD indicates the mass number of the nucleus in the DD experiment, whereas the sum over A runs over the elements in the Sun, $w^2 = v^2 + u_\text{esc}^2(r)$, and

$$\mathcal{H}_A(E_R, r) \equiv \int_{E_\text{min}(v)}^{E_\text{max}(v)} h_A(E_R) dE_R\,. \tag{B.4}$$

JCAP05(2015)036

Eq. (B.3) corresponds to the lower bound on the capture rate if the scattering cross section can be factorized according to eq. (B.1). For certain models such a factorization may not be possible. Generalizing our bound to those cases is beyond the scope of this paper and we leave it for future work.

References

[1] DAMA, LIBRA collaboration, R. Bernabei et al., *New results from DAMA/LIBRA*, *Eur. Phys. J.* **C 67** (2010) 39 [arXiv:1002.1028] [INSPIRE].

[2] CDMS, EDELWEISS collaboration, Z. Ahmed et al., *Combined Limits on WIMPs from the CDMS and EDELWEISS Experiments*, *Phys. Rev.* **D 84** (2011) 011102 [arXiv:1105.3377] [INSPIRE].

[3] XENON100 collaboration, E. Aprile et al., *Dark Matter Results from 225 Live Days of XENON100 Data*, *Phys. Rev. Lett.* **109** (2012) 181301 [arXiv:1207.5988] [INSPIRE].

[4] PICASSO collaboration, S. Archambault et al., *Constraints on Low-Mass WIMP Interactions on ^{19}F from PICASSO*, *Phys. Lett.* **B 711** (2012) 153 [arXiv:1202.1240] [INSPIRE].

[5] LUX collaboration, D.S. Akerib et al., *First results from the LUX dark matter experiment at the Sanford Underground Research Facility*, *Phys. Rev. Lett.* **112** (2014) 091303 [arXiv:1310.8214] [INSPIRE].

[6] CRESST-II collaboration, G. Angloher et al., *Results on low mass WIMPs using an upgraded CRESST-II detector*, *Eur. Phys. J.* **C 74** (2014) 3184 [arXiv:1407.3146] [INSPIRE].

[7] CDMS collaboration, R. Agnese et al., *Silicon Detector Dark Matter Results from the Final Exposure of CDMS II*, *Phys. Rev. Lett.* **111** (2013) 251301 [arXiv:1304.4279] [INSPIRE].

[8] SuperCDMS collaboration, R. Agnese et al., *Search for Low-Mass Weakly Interacting Massive Particles with SuperCDMS*, *Phys. Rev. Lett.* **112** (2014) 241302 [arXiv:1402.7137] [INSPIRE].

[9] Super-Kamiokande collaboration, S. Desai et al., *Search for dark matter WIMPs using upward through-going muons in Super-Kamiokande*, *Phys. Rev.* **D 70** (2004) 083523 [hep-ex/0404025] [INSPIRE].

[10] Super-Kamiokande collaboration, T. Tanaka et al., *An Indirect Search for WIMPs in the Sun using 3109.6 days of upward-going muons in Super-Kamiokande*, *Astrophys. J.* **742** (2011) 78 [arXiv:1108.3384] [INSPIRE].

[11] IceCube collaboration, M.G. Aartsen et al., *Search for dark matter annihilations in the Sun with the 79-string IceCube detector*, *Phys. Rev. Lett.* **110** (2013) 131302 [arXiv:1212.4097] [INSPIRE].

[12] ANTARES collaboration, S. Adrian-Martinez et al., *First results on dark matter annihilation in the Sun using the ANTARES neutrino telescope*, *JCAP* **11** (2013) 032 [arXiv:1302.6516] [INSPIRE].

[13] Super-Kamiokande collaboration, K. Choi et al., *Search for neutrinos from annihilation of captured low-mass dark matter particles in the Sun by Super-Kamiokande*, *Phys. Rev. Lett.* **114** (2015) 141301 [arXiv:1503.04858] [INSPIRE].

[14] M. Kamionkowski, K. Griest, G. Jungman and B. Sadoulet, *Model independent comparison of direct versus indirect detection of supersymmetric dark matter*, *Phys. Rev. Lett.* **74** (1995) 5174 [hep-ph/9412213] [INSPIRE].

[15] L. Bergstrom, J. Edsjo and P. Gondolo, *Indirect detection of dark matter in KM size neutrino telescopes*, *Phys. Rev.* **D 58** (1998) 103519 [hep-ph/9806293] [INSPIRE].

[16] P. Ullio, M. Kamionkowski and P. Vogel, *Spin dependent WIMPs in DAMA?*, *JHEP* **07** (2001) 044 [hep-ph/0010036] [INSPIRE].

JCAP05(2015)036

[17] D. Hooper, F. Petriello, K.M. Zurek and M. Kamionkowski, *The New DAMA Dark-Matter Window and Energetic-Neutrino Searches*, *Phys. Rev.* **D 79** (2009) 015010 [arXiv:0808.2464] [INSPIRE].

[18] G. Wikstrom and J. Edsjo, *Limits on the WIMP-nucleon scattering cross-section from neutrino telescopes*, *JCAP* **04** (2009) 009 [arXiv:0903.2986] [INSPIRE].

[19] R. Kappl and M.W. Winkler, *New Limits on Dark Matter from Super-Kamiokande*, *Nucl. Phys.* **B 850** (2011) 505 [arXiv:1104.0679] [INSPIRE].

[20] C. Arina, G. Bertone and H. Silverwood, *Complementarity of direct and indirect Dark Matter detection experiments*, *Phys. Rev.* **D 88** (2013) 013002 [arXiv:1304.5119] [INSPIRE].

[21] Z.-L. Liang and Y.-L. Wu, *Direct detection and solar capture of spin-dependent dark matter*, *Phys. Rev.* **D 89** (2014) 013010 [arXiv:1308.5897] [INSPIRE].

[22] T. Bruch, A.H.G. Peter, J. Read, L. Baudis and G. Lake, *Dark Matter Disc Enhanced Neutrino Fluxes from the Sun and Earth*, *Phys. Lett.* **B 674** (2009) 250 [arXiv:0902.4001] [INSPIRE].

[23] K. Choi, C. Rott and Y. Itow, *Impact of the dark matter velocity distribution on capture rates in the Sun*, *JCAP* **05** (2014) 049 [arXiv:1312.0273] [INSPIRE].

[24] P.D. Serpico and G. Bertone, *Astrophysical limitations to the identification of dark matter: indirect neutrino signals vis-a-vis direct detection recoil rates*, *Phys. Rev.* **D 82** (2010) 063505 [arXiv:1006.3268] [INSPIRE].

[25] B.J. Kavanagh, M. Fornasa and A.M. Green, *Probing WIMP particle physics and astrophysics with direct detection and neutrino telescope data*, arXiv:1410.8051 [INSPIRE].

[26] P.J. Fox, J. Liu and N. Weiner, *Integrating Out Astrophysical Uncertainties*, *Phys. Rev.* **D 83** (2011) 103514 [arXiv:1011.1915] [INSPIRE].

[27] P.J. Fox, G.D. Kribs and T.M.P. Tait, *Interpreting Dark Matter Direct Detection Independently of the Local Velocity and Density Distribution*, *Phys. Rev.* **D 83** (2011) 034007 [arXiv:1011.1910] [INSPIRE].

[28] M.W. Goodman and E. Witten, *Detectability of Certain Dark Matter Candidates*, *Phys. Rev.* **D 31** (1985) 3059 [INSPIRE].

[29] A.K. Drukier, K. Freese and D.N. Spergel, *Detecting Cold Dark Matter Candidates*, *Phys. Rev.* **D 33** (1986) 3495 [INSPIRE].

[30] K. Freese, J.A. Frieman and A. Gould, *Signal Modulation in Cold Dark Matter Detection*, *Phys. Rev.* **D 37** (1988) 3388 [INSPIRE].

[31] C. McCabe, *DAMA and CoGeNT without astrophysical uncertainties*, *Phys. Rev.* **D 84** (2011) 043525 [arXiv:1107.0741] [INSPIRE].

[32] C. McCabe, *The Astrophysical Uncertainties Of Dark Matter Direct Detection Experiments*, *Phys. Rev.* **D 82** (2010) 023530 [arXiv:1005.0579] [INSPIRE].

[33] M.T. Frandsen, F. Kahlhoefer, C. McCabe, S. Sarkar and K. Schmidt-Hoberg, *Resolving astrophysical uncertainties in dark matter direct detection*, *JCAP* **01** (2012) 024 [arXiv:1111.0292] [INSPIRE].

[34] J. Herrero-Garcia, T. Schwetz and J. Zupan, *On the annual modulation signal in dark matter direct detection*, *JCAP* **03** (2012) 005 [arXiv:1112.1627] [INSPIRE].

[35] J. Herrero-Garcia, T. Schwetz and J. Zupan, *Astrophysics independent bounds on the annual modulation of dark matter signals*, *Phys. Rev. Lett.* **109** (2012) 141301 [arXiv:1205.0134] [INSPIRE].

[36] E. Del Nobile, G.B. Gelmini, P. Gondolo and J.-H. Huh, *Halo-independent analysis of direct detection data for light WIMPs*, *JCAP* **10** (2013) 026 [arXiv:1304.6183] [INSPIRE].

JCAP05(2015)036

[37] E. Del Nobile, G. Gelmini, P. Gondolo and J.-H. Huh, *Generalized Halo Independent Comparison of Direct Dark Matter Detection Data*, *JCAP* **10** (2013) 048 [arXiv:1306.5273] [INSPIRE].

[38] N. Bozorgnia, J. Herrero-Garcia, T. Schwetz and J. Zupan, *Halo-independent methods for inelastic dark matter scattering*, *JCAP* **07** (2013) 049 [arXiv:1305.3575] [INSPIRE].

[39] P.J. Fox, Y. Kahn and M. McCullough, *Taking Halo-Independent Dark Matter Methods Out of the Bin*, *JCAP* **10** (2014) 076 [arXiv:1403.6830] [INSPIRE].

[40] B. Feldstein and F. Kahlhoefer, *Quantifying (dis)agreement between direct detection experiments in a halo-independent way*, *JCAP* **12** (2014) 052 [arXiv:1409.5446] [INSPIRE].

[41] J.F. Cherry, M.T. Frandsen and I.M. Shoemaker, *Halo Independent Direct Detection of Momentum-Dependent Dark Matter*, *JCAP* **10** (2014) 022 [arXiv:1405.1420] [INSPIRE].

[42] N. Bozorgnia and T. Schwetz, *What is the probability that direct detection experiments have observed Dark Matter?*, *JCAP* **12** (2014) 015 [arXiv:1410.6160] [INSPIRE].

[43] M. Drees and C.-L. Shan, *Reconstructing the Velocity Distribution of WIMPs from Direct Dark Matter Detection Data*, *JCAP* **06** (2007) 011 [astro-ph/0703651] [INSPIRE].

[44] W.H. Press and D.N. Spergel, *Capture by the sun of a galactic population of weakly interacting massive particles*, *Astrophys. J.* **296** (1985) 679 [INSPIRE].

[45] K. Griest and D. Seckel, *Cosmic Asymmetry, Neutrinos and the Sun*, *Nucl. Phys.* **B 283** (1987) 681 [INSPIRE].

[46] A. Gould, *WIMP Distribution in and Evaporation From the Sun*, *Astrophys. J.* **321** (1987) 560 [INSPIRE].

[47] A.H.G. Peter, *Dark matter in the solar system II: WIMP annihilation rates in the Sun*, *Phys. Rev.* **D 79** (2009) 103532 [arXiv:0902.1347] [INSPIRE].

[48] A. Serenelli, S. Basu, J.W. Ferguson and M. Asplund, *New Solar Composition: The Problem With Solar Models Revisited*, *Astrophys. J.* **705** (2009) L123 [arXiv:0909.2668] [INSPIRE].

[49] G. Busoni, A. De Simone and W.-C. Huang, *On the Minimum Dark Matter Mass Testable by Neutrinos from the Sun*, *JCAP* **07** (2013) 010 [arXiv:1305.1817] [INSPIRE].

[50] M. Blennow, J. Edsjo and T. Ohlsson, *Neutrinos from WIMP annihilations using a full three-flavor Monte Carlo*, *JCAP* **01** (2008) 021 [arXiv:0709.3898] [INSPIRE].

[51] M. Cirelli et al., *Spectra of neutrinos from dark matter annihilations*, *Nucl. Phys.* **B 727** (2005) 99 [hep-ph/0506298] [INSPIRE].

[52] J. Lavalle and S. Magni, *Making sense of the local Galactic escape speed estimates in direct dark matter searches*, *Phys. Rev.* **D 91** (2015) 023510 [arXiv:1411.1325] [INSPIRE].

[53] A.R. Zentner, *High-Energy Neutrinos From Dark Matter Particle Self-Capture Within the Sun*, *Phys. Rev.* **D 80** (2009) 063501 [arXiv:0907.3448] [INSPIRE].

[54] S. Nussinov, L.-T. Wang and I. Yavin, *Capture of Inelastic Dark Matter in the Sun*, *JCAP* **08** (2009) 037 [arXiv:0905.1333] [INSPIRE].

[55] A. Menon, R. Morris, A. Pierce and N. Weiner, *Capture and Indirect Detection of Inelastic Dark Matter*, *Phys. Rev.* **D 82** (2010) 015011 [arXiv:0905.1847] [INSPIRE].

[56] J. Shu, P.-f. Yin and S.-h. Zhu, *Neutrino Constraints on Inelastic Dark Matter after CDMS II*, *Phys. Rev.* **D 81** (2010) 123519 [arXiv:1001.1076] [INSPIRE].

[57] D.C. Malling et al., *After LUX: The LZ Program*, arXiv:1110.0103 [INSPIRE].

[58] DARWIN Consortium collaboration, L. Baudis, *DARWIN: dark matter WIMP search with noble liquids*, *J. Phys. Conf. Ser.* **375** (2012) 012028 [arXiv:1201.2402] [INSPIRE].

JCAP05(2015)036

[59] XENON1T collaboration, E. Aprile, *The XENON1T Dark Matter Search Experiment*, *Springer Proc. Phys.* **C12-02-22** (2013) 93 [arXiv:1206.6288] [INSPIRE].

[60] SUPERCDMS collaboration, P. Brink, *Conceptual Design for SuperCDMS SNOLAB*, *J. Low. Temp. Phys.* **167** (2012) 1093.

[61] B. Loer, *SuperCDMS SNOLAB*, talk at *Dark Matter 2014*, UCLA, Los Angeles U.S.A. (2014), http://www.pa.ucla.edu/sites/default/files/webform/loer_cdms_UCLA2014v2.pdf.

[62] A. Ibarra, M. Totzauer and S. Wild, *Higher order dark matter annihilations in the Sun and implications for IceCube*, *JCAP* **04** (2014) 012 [arXiv:1402.4375] [INSPIRE].

[63] W.-L. Guo, Z.-L. Liang and Y.-L. Wu, *Direct detection and solar capture of dark matter with momentum and velocity dependent elastic scattering*, *Nucl. Phys.* **B 878** (2014) 295 [arXiv:1305.0912] [INSPIRE].

[64] ICECUBE PINGU collaboration, M.G. Aartsen et al., *Letter of Intent: The Precision IceCube Next Generation Upgrade (PINGU)*, arXiv:1401.2046 [INSPIRE].

[65] KM3NET, *A multi-km3 sized Neutrino Telescope*, http://www.km3net.org/home.php.

[66] K. Abe et al., *Letter of Intent: The Hyper-Kamiokande Experiment — Detector Design and Physics Potential —*, arXiv:1109.3262 [INSPIRE].

[67] V.A. Bednyakov and F. Simkovic, *Nuclear spin structure in dark matter search: The Finite momentum transfer limit*, *Phys. Part. Nucl.* **37** (2006) S106 [hep-ph/0608097] [INSPIRE].

[68] P. Toivanen, M. Kortelainen, J. Suhonen and J. Toivanen, *Large-scale shell-model calculations of elastic and inelastic scattering rates of lightest supersymmetric particles (LSP) on I-127, Xe-129, Xe-131 and Cs-133 nuclei*, *Phys. Rev.* **C 79** (2009) 044302 [INSPIRE].

[69] D.G. Cerdeno, M. Fornasa, J.-H. Huh and M. Peiro, *Nuclear uncertainties in the spin-dependent structure functions for direct dark matter detection*, *Phys. Rev.* **D 87** (2013) 023512 [arXiv:1208.6426] [INSPIRE].

[70] P. Klos, J. Menéndez, D. Gazit and A. Schwenk, *Large-scale nuclear structure calculations for spin-dependent WIMP scattering with chiral effective field theory currents*, *Phys. Rev.* **D 88** (2013) 083516 [arXiv:1304.7684] [INSPIRE].

[71] XENON100 collaboration, E. Aprile et al., *Limits on spin-dependent WIMP-nucleon cross sections from 225 live days of XENON100 data*, *Phys. Rev. Lett.* **111** (2013) 021301 [arXiv:1301.6620] [INSPIRE].

[72] K.M. Zurek, *Asymmetric Dark Matter: Theories, Signatures and Constraints*, *Phys. Rept.* **537** (2014) 91 [arXiv:1308.0338] [INSPIRE].

[73] N. Bozorgnia and T. Schwetz, *Is the effect of the Sun's gravitational potential on dark matter particles observable?*, *JCAP* **08** (2014) 013 [arXiv:1405.2340] [INSPIRE].

JCAP05(2015)036